A&A 439, 387–399 (2005)
DOI: 10.1051/0004-6361:20052641


Astronomy & Astrophysics

# Absolute cross sections for *L*-shell photoionization of the ions $N^{2+}$, $N^{3+}$, $O^{3+}$, $O^{4+}$, $F^{3+}$, $F^{4+}$ and $Ne^{4+}$⋆

J.-M. Bizau[1], J.-P. Champeaux[1], D. Cubaynes[1], F. J. Wuilleumier[1], F. Folkmann[2], T. S. Jacobsen[2], F. Penent[3], C. Blancard[4], and H. Kjeldsen[2]

[1] Laboratoire d'Interaction des Rayons X avec la Matière (LIXAM), UMR 8624 du CNRS, University Paris-Sud, Bât. 350, 91405 Orsay, France
e-mail: jean-marc.bizau@lixam.u-psud.fr
[2] Department of Physics and Astronomy, University of Aarhus, 8000 Aarhus C, Denmark
e-mail: kjeldsen@phys.au.dk
[3] Laboratoire de Chimie Physique- Matière et Rayonnement (LCP-MR), Université Pierre et Marie Curie, 11 rue Pierre et Marie Curie, 75231 Paris Cedex 05, France
[4] CEA/DAM Ile-de-France, Département de Physique Théorique et Appliquée, BP 12, 91680 Bruyères-le-Châtel, France

Received 5 January 2005 / Accepted 4 February 2005

**Abstract.** Absolute photoionization cross sections for the ions $N^{2+}$, $N^{3+}$, $O^{3+}$, $O^{4+}$, $F^{3+}$, $F^{4+}$ and $Ne^{4+}$ are measured using the merged-beam technique, combining the synchrotron radiation from an undulator at the storage ring ASTRID with ions produced by an ECR ion source. The spectral structures and the development of the cross sections along iso-electronic sequences are discussed. The experimental data are compared with *R*-matrix calculations from the Opacity Project and other sources, MCDF calculations, as well as the model functions provided by Verner et al. (1996). In general, good agreement between experiment and calculations is observed for the magnitude of the continuum cross sections whereas very significant discrepancies are present for the resonance structures. The experimental data are also available in electronic form at the CDS.

**Key words.** atomic data – atomic processes – line: identification

## 1. Introduction

Photoionization is a fundamental atomic process that plays important roles in many physical systems, including a broad range of astrophysical objects as diverse as QSOs, the atmosphere of hot stars, protoplanetary nebula, HII regions, novae and supernovae. Therefore, absolute photoionization cross sections are required to model such systems, and it is an important task for the atomic-physics community to provide the data. Among the most relevant species for astrophysics are the elements C, N, O and their ions, but heavier elements are also important, for example Fe.

The photoionization cross sections used for modeling of astrophysical systems have generally been provided by calculations, because no experimental data were available. As a consequence, significant effort has been put into improving the quality of calculated data. In this context the Opacity Project (Seaton 1987; The Opacity Project Team 1995) deserves special attention, being the first major project providing large quantities of data using the advanced *R*-matrix method in combination with the close-coupling approximation (Berrington et al. 1977). However, in general these calculations have not been tested by experiment, and this remains an urgent task.

It is challenging to measure absolute photoionization cross sections. For neutral atoms, the difficulties related to the determination of the target density have limited the data available to the noble gases and a few other isolated systems. In the case of ions, the merged-beam technique which is characterized by colinearly overlapping beams of ions and photons can yield absolute data, because the density of an ion beam can be determined directly. However, the fact that the density of ions in a target beam is low ($\sim 10^6/\mathrm{cm}^3$) implies that a very high photon flux is required. The merged-beam technique was first used for photoionization studies by Lyon et al. (1986), but the measurements were limited to large cross sections, because synchrotron radiation from bending magnets was used.

With the increased flux of VUV photons becoming available due to the construction of undulator beam lines at synchrotron radiation facilities it has become possible to measure smaller cross sections. In consequence, the number of ions for which cross-section data are available is increasing rapidly, with experiments being performed in Denmark

⋆ Complete data set mentioned in Sect. 4 is only available in electronic form at the CDS via anonymous ftp to cdsarc.u-strasbg.fr (130.79.128.5) or via http://cdsweb.u-strasbg.fr/cgi-bin/qcat?J/A+A/439/387

(ASTRID, Kjeldsen et al. 1999b), France (SuperACO, Bizau et al. 2000), Japan (Photon Factory, Koizumi et al. 1995; SPring-8, Yamaoka et al. 2002) and USA (ALS, Covington et al. 2001). For a review of the previous works, see West (2001). In particular, the experiments performed on *L*-shell photoionization include the ions $B^+$ (Schippers et al. 2003), $C^+$ (Kjeldsen et al. 1999a, 2001), $C^{2+}$ (Müller et al. 2002), $N^+$ (Kjeldsen et al. 2002a), $O^+$ (Kjeldsen et al. 2002a; Covington et al. 2001; Aguilar et al. 2003), $O^{2+}$ – $O^{4+}$ (Champeaux et al. 2003), and $Ne^+$ (Covington et al. 2002). In most of these studies absolute cross sections have been measured and often good agreement was found with the results of *R*-matrix calculations.

In the present project, the merged-beam technique was used to measure absolute photoionization cross sections for a number of light multiply charged ions of astrophysical relevance: $N^{2+}$, $N^{3+}$, $O^{3+}$, $O^{4+}$, $F^{3+}$, $F^{4+}$ and $Ne^{4+}$. The principal motivations were to test the *R*-matrix calculations of the Opacity Projects TOPbase (see Cunto et al. 1993, data downloaded from at `http://heasarc.gsfc.nasa.gov/topbase/topbase.html`) and to follow the development of the cross sections along iso-electronic sequences. In addition, the experimental data are compared with MCDF calculation (partly obtained within the present investigation) as well as the model functions provided by Verner et al. (1996), and the spectral structures are discussed. As it will be made apparent below, very significant deviations between the experimental data and the *R*-matrix calculations from the Opacity Project are present concerning the spectral structure for some of the ions studied.

## 2. Experimental

The experiments were performed using the merged-beam technique with the photons being emitted by the undulator in the storage ring ASTRID at the University of Aarhus and the ion beam extracted from an ECR (Electron Cyclotron Resonance) ion source. The set-up is sketched in Fig. 1 and described in detail in Kjeldsen et al. (2005). In brief, a $q \times 2$ kV beam of the target ions with charge state $q$ was merged colinearly with the photons over a distance of 50 cm. The photoionized ions with charge state $q + 1$ were subsequently separated magnetically from the target ions, and the two species were detected by a particle detector (D1) and a Faraday cup (FC2), respectively (see Fig. 1).

The apparatus described by Kjeldsen et al. (1999b, 2001) was modified prior to the present experiment. Most important, a 10 GHz all permanent magnet ECR ion source (Bizau et al. 2003) was installed. The source was developed by CEA Grenoble and has previously been used in similar experiments at the storage ring SuperACO (Bizau et al. 2000, 2001, 2003; Champeaux et al. 2003). The ion beam line was shortened and the ion optics simplified near the ion source in order to make space available for the ECR source, reduce space-charge effects and simplify the optimization. A new Faraday cup (FC2 in Fig. 1) to detect the target ion beam was installed (the Faraday cup FC3 to detect negative target ions was also added, see Kjeldsen et al. 2004). FC2 was necessary because the original Faraday cup (FC1) was designed for singly charged ions

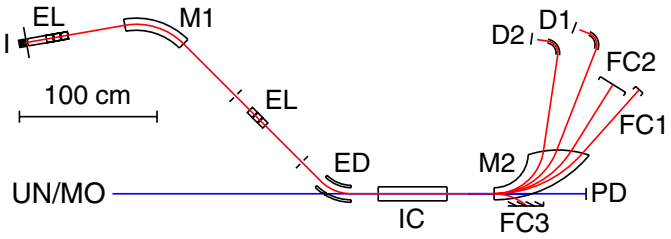


**Fig. 1.** The experimental set-up. UN/MO: photon beam from the undulator/Miyake-monochromator beam line at the ASTRID storage ring; I: ECR ion source; EL: Einzel lens; M1 and M2: deflection magnets; ED: Electrostatic deflector; IC: interaction chamber (biased); FC1, FC2 and FC3: Faraday cups; PD: calibrated photodiode; D1 and D2: particle detectors. FC1, FC3 (for negative ions) and D2 were not used in the present experiments.

and was too far from the detector (D1) for simultaneous detection of target ions and photoionized ions with charge-states $q$ and $q + 1$, respectively, for $q > 2$. The measurements were performed with an acceleration voltage of 2 kV and a decelerating bias on the interaction chamber of +800 V, +900 V and +1000 V for the target-ion charge stages $q = +2$, +3, and +4, respectively; for comparison +600 V was used for $q = +1$ and +300 V (accelerating) for $q = -1$. The increasing bias was needed in order to distinguish the energy-marked ionized ions created inside the 50 cm long interaction region (final energy = 9.0 keV in the case of $+4 \rightarrow +5$ experiments) from the ions created outside of this region (energy = 8.0 keV), thereby ensuring a proper determination of the interaction length.

The cross-section measurements were made absolute using the current of the target-ion beam, the photon-beam intensity (measured by a calibrated $Al_2O_3$ photodiode), the ion- and photon-beam profiles (measured using scanning slits), the velocity of the target ions, the photoionization signal, the efficiency of the particle detector and the known length of the interaction region. The particle detector (D1: Johnston multiplier type MM1-1SG) was calibrated by $N^{3+}$, $N^{4+}$ and $N^{5+}$ ions yielding efficiencies of 67.6%, 70.5% and 71.4%, respectively. The currents of target ions in the interaction chamber were in the range of 50–200 nA. Ground-state ions generally constituted the majority of the target ions, but significant quantities of metastable ions from the ECR source were also present, constituting as much as 50% in one case. The calibration of the photodiode was performed using Ne gas in an ionization chamber, and the photon-energy calibration was made in the same chamber using autoionizing resonances in He (Domke et al. 1996) and Kr (NIST 1999, $3d \rightarrow 5p$) observed in first and second order.

The results presented in this paper clearly demonstrate that experiments become more difficult with increasing charge stage $q$ of the target ions. Generally, the ion-beam current extracted from the ECR ion source with a fixed acceleration voltage decreases only slowly with increasing $q$, however the increased velocity and charge stage will result in a decrease of the density of target ions in the reaction zone (and consequently also of the photoionization signal) proportional to $q^{-3/2}$ for a fixed current. The background signal, on the other hand, may still be large. Finally, the photon flux in many cases decreases

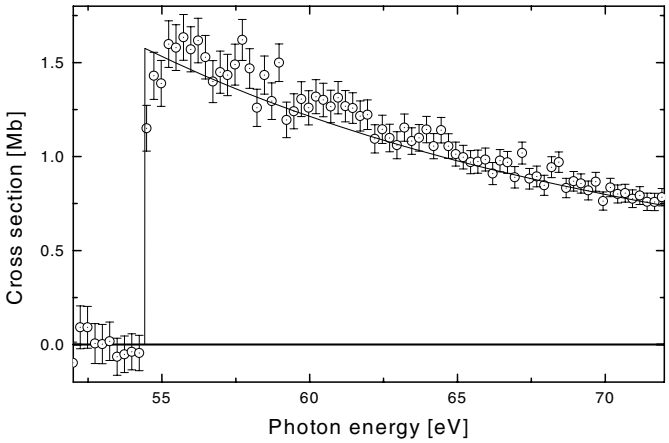


**Fig. 2.** The photoionization cross section of $^3He^+$ ions – a test of the experimental accuracy. Theory: line; absolute cross section measurement: circles and statistical error bars.

as a result of the increasing photon energy necessary for investigations of multiply charged ions.

The accuracy of the experimental cross sections reported from these investigations is estimated to be about ±15% and is dominated by the uncertainty in the determination of the absolute photon flux (5–10%), followed by the uncertainties resulting from the measurements of the sizes and overlap of the merging beams (2–5%) and the detector efficiencies (1–3%). With the purpose of testing the obtained accuracy we have measured the absolute photoionization cross section for $He^+$ ions. Figure 2 shows the result and a comparison with the established theoretical cross section (Sobelman 1992, and references therein). The measured cross section follows the theoretical one over the entire photon-energy range studied, and the deviation is of the order of 5%, thus increasing confidence in the claimed accuracy of the cross sections reported.

## 3. MCDF calculations

To interpret our experimental data, we performed MCDF calculations using the code developed by Bruneau (1984). All calculations were performed assuming that the K shell is filled. For photoexcitation cross sections of C-like ions we included 1532 levels issued from the 60 following configurations: $[2s2p]^4$ and $[2s2p]^3nl$. For B-like ions, we considered 985 levels issued from the 84 configurations $[2s2p]^3$ and $[2s2p]^2nl$. For Be-like ions 265 levels were included from the 45 following configurations: $[2s2p]^2$ and $[2s2p]nl$. For C- and Be-like ions $3 \le n \le 9$ and $0 \le l \le 2$, for B-like ions $n$ goes up to 11. For all ions, photoexcitation cross sections from the ground and the first excited metastable levels have been computed assuming Lorentzian profiles with a full width at half maximum (*FWHM*) of 0.01 eV for the shape of all excitation lines present in the experimentally investigated photon energy range.

To calculate the direct photoionization cross sections we considered the following configurations: $[2s2p]^x$, $[2s2p]^{(x-1)}$, where $x$ equals 4, 3, and 2 for C-, B-, and Be-like ions respectively, except for $N^{3+}$ where only the configuration $[2s]^1$ was introduced. For each level constructed on the $[2s2p]^x$ configurations we calculated the photoionization cross sections at regular intervals on the photon energy scale (typically every 1 eV). The first energy was chosen near the ionization threshold and the last one 30 eV above. Then the cross section was fitted to a function of the form $A \cdot (I/h\nu)^B$, where $I$ was the threshold energy. $A$ and $B$ were the adjustable parameters of the fit. For both photoexcitation and photoionization cross sections we used the length-form of the electric-dipole operator. For each initial level, we calculated the total photoionization cross section as a sum of the photoexcitation and photoionization cross sections, i.e. the interference between the two pathways were not taken into account.

To compare our theoretical results with our experimental spectra, we constructed a synthetic spectrum as a weighted sum of individual total photoionization cross sections of the different initial states populated in the experiments. In addition, the theoretical results were convoluted with a Gaussian function with a *FWHM* corresponding to the averaged spectral resolution.

## 4. Results

Absolute photoionization cross section have been obtained for the Be-like ions $N^{3+}$ (photon-energy range 62–89 eV) and $O^{4+}$ (100–130 eV), the B-like ions $N^{2+}$ (39–138 eV), $O^{3+}$ (65–99 eV) and $F^{4+}$ (100–140 eV), and the C-like ions $F^{3+}$ (75–110 eV) and $Ne^{4+}$ (110–170 eV). In the following the experimental data are compared with MCDF calculations and with *R*-matrix calculations from the Opacity Project and other sources. In addition, the spectral structure is discussed. The discussion is divided into groups of iso-electronic ions in order to follow the effect of the nuclear charge $Z$ on the spectral structure and the continuum cross section. Also, this division facilitates the discussion. The emphasis will be on the threshold regions, but the complete data sets can be obtained at `http://www.phys.au.dk/amo/atomphys/atomphys.htm`

### 4.1. B-like ions: $N^{2+}$, $O^{3+}$ and $F^{4+}$

In addition to the data for $N^{2+}$, $O^{3+}$ and $F^{4+}$ obtained as part of the present investigation and shown in Figs. 3–5, data were previously obtained for $C^+$ (Kjeldsen et al. 1999a, 2001), $N^{2+}$ (Bizau et al. 2004, only relative data) and $O^{3+}$ (Champeaux et al. 2003). In the last two cases the data were measured utilizing a different set-up at the storage ring SuperACO. Those data exhibit good agreement with the present ones. Also shown in Fig. 3 are simulated spectra (middle and lower panels) obtained from weighted sums of the different calculated cross sections of the respective $2s^22p\ ^2P$ ground states and $2s2p^2\ ^4P$ metastable states. The weights correspond to the populations of the different states in the experiments and were determined by comparing calculated and measured data (see below). The calculated spectra have been folded with 100, 250 and 500 meV Gaussian profiles (*FWHM*) which represent the experimental resolution in the case of $N^{2+}$, $O^{3+}$, and $F^{4+}$, respectively. The *R*-matrix results (middle panels) are from Fernley et al. (1999, from the Opacity Project) and Nahar & Pradhan (1997), with additional data for $O^{3+}$ in Fig. 5 by Nahar (1998, 2004). MCDF

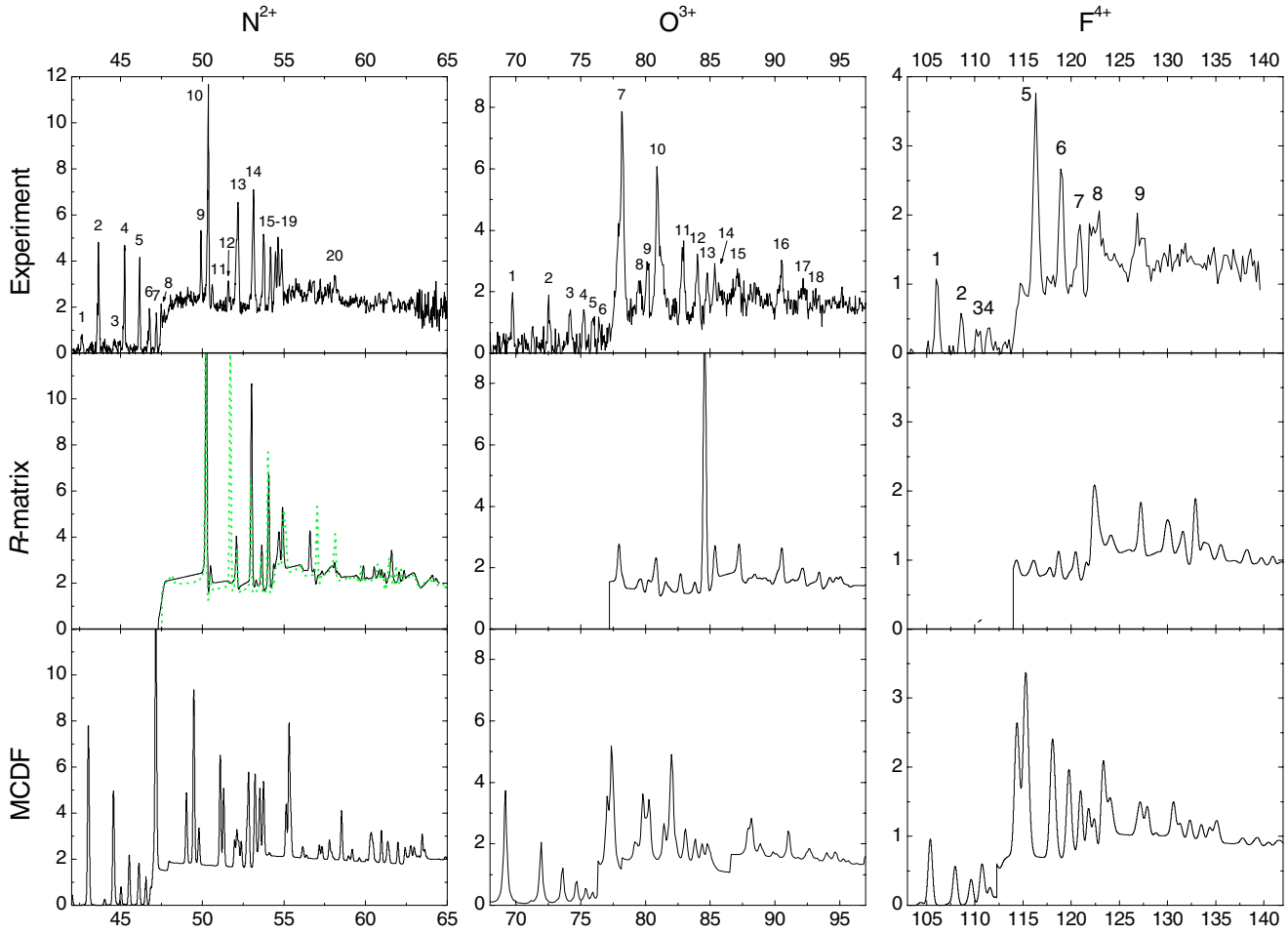


**Fig. 3.** The absolute photoionization cross sections (in Mb = $10^{-18}$ cm$^2$) as a function of the photon energy (eV) for the B-like ions $N^{2+}$ (*left*), $O^{3+}$ (*center*) and $F^{4+}$ (*right*). *Top*: present experimental data; *middle*: *R*-matrix calculations; *bottom*: MCDF calculations. The *R*-matrix data by Fernley et al. (1999, obtained from the Opacity Projects TOPbase) are shown by the (black) solid line, whereas newer data for $N^{2+}$ (Nahar & Pradhan 1997) are shown by the (green) dotted line. The theoretical spectra have been convoluted with Gaussians of 100, 250 and 500 meV (*FWHM*), respectively, and are calculated under the assumption of a ($^4$P:$^2$P) fraction of (0.90:0.10) for $N^{2+}$ and $F^{4+}$ and (0.84:0.16) for $O^{3+}$. The MCDF data are from the present work ($N^{2+}$ and $F^{4+}$) or by Champeaux et al. (2003, $O^{3+}$). The numbers refer to Tables 2–4. The experimental data for $N^{2+}$ and $O^{3+}$ are shown enlarged in Figs. 4 and 5, respectively.

calculations (lower panels) for $N^{2+}$ and $F^{4+}$ are from the present work, whereas $O^{3+}$ calculations are by Champeaux et al. (2003).

The experimental spectra show different resonances superimposed on decreasing continua and exhibit marked differences along the series $N^{2+}$ – $F^{4+}$. A continuous decrease of the continuum cross section is observed going through the series while the ionization threshold increases. The thresholds for $2s^22p\ ^2P$ ground-state ions are measured at 47.5 eV, 77.3 eV and 114.27 eV, respectively, which is close to the values reported in NIST (1999) and shown in Table 1 together with the energies obtained from our MCDF calculations. The observation of resonances below the ionization thresholds attests to the presence of target ions in the $2s2p^2\ ^4P$ metastable state in the experiment.

In principle, all these spectra utilize the same constituents, and the gross features of the resonance structure indeed look similar for all the ions of the sequence. Nevertheless, significant changes are observed. The allowed one-electron transitions involving 2s electrons are $2s^22p\ ^2P + h\nu \rightarrow 2s2p(^{1,3}P)np\ ^2S,\ ^2P,\ ^2D$. The $^2P$ terms cannot Coulomb autoionize into the $1s^22s^2\ ^1S + \epsilon p$ continuum, however previous studies (see e.g. Kjeldsen et al. 1999a) showed that these states were indeed responsible for peaks in the photoionization spectrum, and their presence has been attributed to the influence of relativistic effects in the case of $C^+$ (Kjeldsen et al. 2001). Thus, we can expect the presence of 6 Rydberg series converging to the $^1P$ and $^3P$ limits of the 2s2p core. In addition, resonances originating from metastable target ions are responsible for the resonances below threshold. The involved transitions are $2s2p^2\ ^4P + h\nu \rightarrow 2s2p(^3P)\ ns\ ^4P,\ nd\ ^4P,\ ^4D$ as shown by the MCDF calculations. These 3 Rydberg series all converge to the energy limit at $E(2s2p\ ^3P) - E(2s2p^2\ ^4P)$, and their presence must be due to autoionization through relativistic effects. The different Rydberg series are indicated in Figs. 4 and 5 for $N^{2+}$ and $O^{3+}$, respectively, and the measured and calculated energies of the observed peaks together with their assignments are summarized in Tables 2–4.

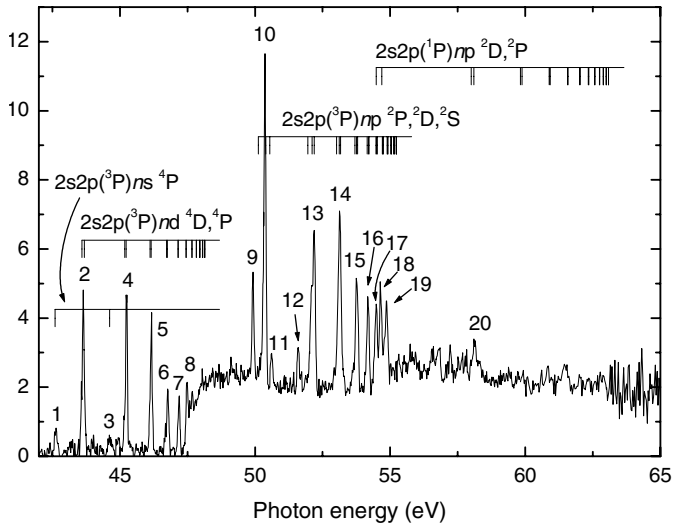


**Fig. 4.** The measured photoionization cross sections of $N^{2+}$ with the different Rydberg series indicated. The numbers refer to Table 2. The Rydberg series are extrapolated utilizing the series limits and lower-lying members with known energy (NIST 1999).

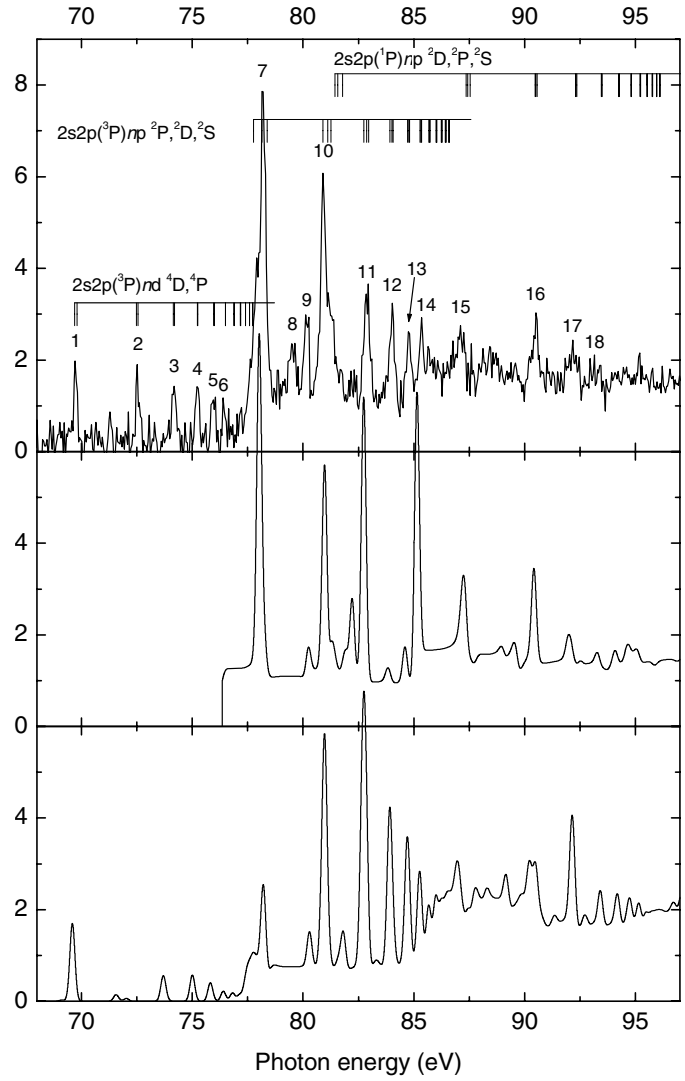


**Fig. 5.** The measured photoionization cross sections of $O^{3+}$ with the different Rydberg series indicated (*top graph*). The numbers refer to Table 3. The Rydberg series are extrapolated utilizing the series limits and lower-lying members with known energy (NIST 1999). Also shown are the *R*-matrix calculations from Nahar (1998, *middle*) and Nahar (2004, *bottom*). The theoretical spectra have been convoluted with Gaussians of 250 meV (*FWHM*) and are calculated under the assumption of a 16% fraction of ions in the metastable states.

The experimental spectrum of $N^{2+}$ is taken with the best resolution and therefore reveals the most structure. The spectrum is shown in Fig. 3 and in more detail in Fig. 4, while the energy and the assignments of the most intense peaks are given in Table 2. The present assignments are equal to those obtained from NIST (1999) and are in good agreement with the MCDF calculations, except for some lines. Our MCDF calculations predict a crossing of the $^2$D and $^2$P terms of the 2s2p($^3$P)*n*p series at $n = 8$. The calculated energy of the 2s2p($^3$P)*n*p resonances is lower by about 0.9 eV whereas the 2s2p($^1$P)*n*p resonances are higher by about 0.5 eV. The reason for the difference between the two series is that the method does not predict the splitting between the 2s2p $^1$P and $^3$P terms correctly for this ion, see Table 1. This implies that the configuration interaction between 2s2p($^3$P)*n*p and 2s2p($^1$P)*n*p is not described correctly. The problem should be kept in mind when comparing experimental data with data obtained by an ab initio calculation such as the *R*-matrix method or MCDF calculations, as discussed by Kjeldsen et al. (1999a, 2001). The assignment of peak No. 12 is difficult. It can be identified from NIST as the $2p^2(^3P)3d\ ^2D$ two-electron transition from the ground state, but our MCDF calculations predict this term to be at 55.44 eV. Note that Coulomb autoionization of this state is forbidden. In the same way, the assignment of the peaks labeled 17–19 is not straightforward since there will be some degree of configuration interaction between the 2s2p($^3$P)($n \geq 10$)p $^2$D, $^2$P, $^2$S and the corresponding 2s2p($^1$P)4p terms. Moreover, additional weak and broad peaks between number 19 and 20, and also at higher energies, do not seem to belong to any of these Rydberg series. They are most likely the result of two-electron transitions, like those observed in the spectrum of $C^+$ by Kjeldsen et al. (1999a, 2001). The peaks below threshold clearly correspond to transitions from the metastable component but the limited resolution does not allow us to resolve the 2s2p($^3$P)*n*d $^4$D, $^4$P excited terms. Similarly, in the case of 2s $\rightarrow$ *n*p transitions from the ground state, it has only been possible to resolve the $^2$P, $^2$D and $^2$S excited terms for $n = 5$.

For $O^{3+}$ (see Figs. 3 and 5) the assignment of the lines is more difficult because of the increasing overlap between the 2s2p($^3$P)*n*p and 2s2p($^1$P)*n*p series and the larger experimental excitation band pass. In the present identifications (Table 3, Figs. 3 and 5), the assignment of the lines 9 and 10 has been reversed compared to those given by Champeaux et al. (2003). The line 10, which is more intense and broad, is likely due to overlapping transitions from the ground state to 2s2p($^3$P)6p $^2$P, $^2$D and 2s2p($^1$P)4p $^2$P, $^2$D. The smaller line No. 9 corresponds then to the double excitation to $2p^2(^3P)3d\ ^2D$, in better agreement with the NIST data (a misprint in Champeaux et al. 2003 has labeled the line No. 10 as $2p^24d\ ^2D$ instead of 3d) and the fact that this excited state is not allowed to Coulomb

**Table 1.** Some relevant energy levels and ionization potentials (in eV) from our MCDF calculations and from NIST (1999) for B-like ions. The energy of each term is obtained as the mean of the energy levels pondered by their statistical weight.

| | $N^{2+}$ | | $O^{3+}$ | | $F^{4+}$ | |
|---|---|---|---|---|---|---|
| Level | MCDF | NIST | MCDF | NIST | MCDF | NIST |
| $2s^2 2p\ ^2P$ | 0 | 0 | 0 | 0 | 0 | 0 |
| $2s2p^2\ ^4P$ | 6.70 | 7.10 | 8.52 | 8.88 | 10.34 | 10.69 |
| $E_{IP}$ ($2s^2\ ^1S$) | 46.92 | 47.45 | 76.14 | 77.41 | 113.96 | 114.24 |
| $E_{IP}$ ($2s2p\ ^3P$) | 53.19 | 55.80 | 86.60 | 87.61 | 123.22 | 126.25 |
| $E_{IP}$ ($1s^2 2s2p\ ^1P$) | 62.41 | 63.65 | 96.93 | 97.10 | 135.82 | 137.41 |
| $\Delta E_{IP}(^1P - ^3P)$ | 9.22 | 7.85 | 10.33 | 9.49 | 12.60 | 11.25 |

**Table 2.** Location and designation of the resonances in the photoionization spectrum of $N^{2+}$. The peak numbers refer to Figs. 3 and 4, and * denotes that the initial state of the transition is the $2s2p^2\ ^4P$ metastable states – otherwise the initial state is the $2s^2 2p\ ^2P$ ground state. When several terms are given the MCDF and NIST (1999) energies correspond to the mean value of the terms energy weighted by their statistical population. The accuracy of the experimental energies listed is about 15 meV.

| Peak | Energy (eV) | | | Final state |
|---|---|---|---|---|
| | Exp. | MCDF | NIST | |
| 1* | 42.62 | 42.03 | 42.61 | $2s2p(^3P)5s\ ^4P$ |
| 2* | 43.64 | 43.02 | 43.61 | $2s2p(^3P)5d\ ^4D, ^4P$ |
| 3* | 44.64 | 44.03 | 44.62 | $2s2p(^3P)6s\ ^4P$ |
| 4* | 45.25 | 44.56 | 45.20 | $2s2p(^3P)6d\ ^4D, ^4P$ |
| 5* | 46.15 | 45.53 | 46.14 | $2s2p(^3P)7d\ ^4D, ^4P$ |
| 6* | 46.75 | 46.13 | 46.75 | $2s2p(^3P)8d\ ^4D, ^4P$ |
| 7* | 47.19 | 46.56 | 47.17 | $2s2p(^3P)9d\ ^4D, ^4P$ |
| 8* | 47.49 | 46.84 | 47.46 | $2s2p(^3P)10d\ ^4D, ^4P$ |
| 9 | 49.93 | 49.02 | 49.93 | $2s2p(^3P)5p\ ^2P$ |
| 10 | 50.37 | 49.48 | 50.37 | $2s2p(^3P)5p\ ^2D$ |
| 11 | 50.61 | 49.81 | 50.61 | $2s2p(^3P)5p\ ^2S$ |
| 12 | 51.61 | | 51.54 | $2p^2(^3P)3d\ ^2D$ |
| 13 | 52.19 { | 51.33 | 52.10 | $2s2p(^3P)6p\ ^2P$ |
| | | 51.11 | 52.21 | $2s2p(^3P)6p\ ^2D$ |
| 14 | 53.14 | 52.11 | 53.13 | $2s2p(^3P)7p\ ^2P, ^2D$ |
| 15 | 53.77 | 52.86 | 53.75 | $2s2p(^3P)8p\ ^2P, ^2D$ |
| 16 | 54.18 | 53.24 | 54.20 | $2s2p(^3P)9p\ ^2P, ^2D$ |
| 17 | 54.49 | 53.53 | 54.51 | $2s2p(^3P)10p\ ^2P, ^2D$ |
| 18 | 54.65 | 55.14 | 54.66 | $2s2p(^1P)4p\ ^2D$ |
| 19 | 54.86 | 55.32 | 54.85 | $2s2p(^1P)4p\ ^2P$ |
| 20 | 58.13 | 58.54 | 58.15 | $2s2p(^1P)5p\ ^2P, ^2D$ |

**Table 3.** Location and designation of the resonances in the photoionization spectrum of $O^{3+}$. See caption to Table 2. The peak numbers refer to Figs. 3 and 5. The accuracy of the experimental energies listed is about 50 meV.

| Peak | Energy (eV) | | | Transition |
|---|---|---|---|---|
| | Exp. | MCDF | NIST | |
| 1* | 69.74 | 69.18 | 69.80 | $2s2p(^3P)5d\ ^4D, ^4P$ |
| 2* | 72.55 | 71.94 | 72.53 | $2s2p(^3P)6d\ ^4D, ^4P$ |
| 3* | 74.18 | 73.60 | 74.15 | $2s2p(^3P)7d\ ^4D, ^4P$ |
| 4* | 75.23 | 74.68 | | $2s2p(^3P)8d\ ^4D, ^4P$ |
| 5* | 75.95 | 75.41 | | $2s2p(^3P)9d\ ^4D, ^4P$ |
| 6* | 76.44 | 75.94 | | $2s2p(^3P)10d\ ^4D, ^4P$ |
| 7 | 78.16 | 77.4 | 78.3 | $2s2p(^3P)5p\ ^2P, ^2D, ^2S$ |
| 8 | 79.53 | | | |
| 9 | 80.16 | 79.82 | 80.20 | $2p^2(^3P)3d\ ^2D$ |
| 10 | ~ 80.9 { | 80.2 | | $2s2p(^3P)6p\ ^2P,^2D,^2S$ |
| | | 82.3 | 81.43 | $2s2p(^1P)4p\ ^2P,^2D,^2S$ |
| 11 | 82.88 | 81.9 | | $2s2p(^3P)7p\ ^2P, ^2D$ |
| 12 | 84.01 | 83.12 | | $2s2p(^3P)8p\ ^2P, ^2D$ |
| 13 | 84.78 | 83.84 | | $2s2p(^3P)9p\ ^2P, ^2D$ |
| 14 | 85.35 | 84.37 | | $2s2p(^3P)10p\ ^2P, ^2D$ |
| 15 | 87.11 | 88.15 | | $2s2p(^1P)5p\ ^2P, ^2D$ |
| 16 | 90.47 | 91.09 | | $2s2p(^1P)6p\ ^2P, ^2D$ |
| 17 | 92.14 | 92.8 | | $2s2p(^1P)7p\ ^2P, ^2D$ |
| 18 | 93.15 | 93.99 | | $2s2p(^1P)8p\ ^2P, ^2D$ |

autoionize. Also, Champeaux et al. assigned the peak at 79.53 eV (No. 8) to the transition from the ground state to the $^2S$ term of the $2s2p(^3P)5p$ configuration, but that would imply a very large splitting between the $^2S$ and $^2D$ terms. Therefore we assign here the $^2S$ term to be part of the unresolved peak at 49.93 eV (No. 7), which leaves peak No. 8 unaccounted for.

The assignment of the observed spectral structure seems apparently easier in the case of $F^{4+}$, and the result is presented in Table 4. Apart from the fact that the lower experimental resolution leaves only the gross features in the spectrum observable, one reason is that in contrast to the situations for $O^{3+}$ and $C^+$ (Kjeldsen et al. 1999a) but similarly to that of $N^{2+}$ there is only little overlap between the members of the $2s2p(^3P)np$ and $2s2p(^1P)np$ Rydberg series. As a consequence, configuration interaction is reduced and simple, non-pertubed Rydberg series are more easily identified.

A comparison of the experimental spectra of the three isoelectronic ions (see Tables 2–4) shows that successive 2s inner sub-shell resonances move downward in energy relative to the threshold when the nuclear charge $Z$ increases. As an example of this, in the case of $N^{2+}$ the $2s2p(^3P)5p\ ^2D$ resonance is located approximately 3 eV above the $2s^2$ ionization threshold, whereas the same resonance is located just at threshold in the $O^{3+}$ spectrum. For $F^{4+}$ it has plunged below the ionization

limit and is therefore not visible, whereas for $C^+$ the 4p resonance is present too. This behavior can be explained by the fact that as $Z \to \infty$ the ions become more and more hydrogen-like, and the splitting between the 2s2p and $2s^2$ configurations consequently becomes smaller (relative to the ionization potential). A downward movement of inner sub-shell resonances with respect to outer-shell thresholds can therefore be expected for all sequences where the outermost sub shell is different to $l = 0$.

As mentioned earlier, the Rydberg states below the ionization threshold of the ground state is used to estimate the fraction of metastable ions in the target ion beams by comparing the oscillator strengths of the resonances with the theoretical values. The series can be followed for $n$-values in the range 5–10 for $N^{2+}$, 5–10 for $O^{3+}$, and 6–9 for $F^{4+}$. The lowest peaks are relatively weak for $N^{2+}$ and $O^{3+}$, probably because the associated final states decay partly by fluorescence and not only autoionization, whereas the higher members decay by autoionization exclusively. Experimental oscillator strengths for the $2s2p(^3P)nd\ ^4D, ^4P$ terms have been obtained by fitting with Gaussian profiles. For the $R$-matrix and MCDF calculations the oscillator strengths for excitation are used directly, i.e. the excited states are assumed to autoionize with 100% probability. The results are presented in Table 5, and it is estimated from the mean value of the ratios obtained for $R$-matrix and MCDF calculations (last 2 columns) that the metastable fractions are 10, 16 and 10%, respectively, for the three ions, which is in agreement with previous results obtained for $N^{2+}$ (8% metastable: Bizau et al. 2004) and $O^{3+}$ (16% metastable: Champeaux et al. 2003) using the same ECR source.

In general, the cross sections for direct photoionization for the different ions decrease in parallel with the photon energy. However, at a given energy there is a small increase in the cross section with increasing $Z$, due to the contraction of the orbitals and the consequently larger overlap between the wave functions. The cross section at the respective ionization thresholds decreases along the series because of the increasing ionization energy. This behavior is in accordance with the work of Msezane et al. (1977) on the development of the cross sections for direct photoionization along the iso-electronic series.

The photoionization cross sections of the B-like ions $N^{2+}$, $O^{3+}$ and $F^{3+}$ have been calculated utilizing the $R$-matrix method by Fernley et al. (1999) as part of the Opacity Project. Employing the same method, Nahar & Pradhan (1997) calculated the cross sections of the ions of C, N, and O (including $N^{2+}$ and $O^{3+}$) as part of the Iron Project, and later Nahar (1998) reported details of the calculations for oxygen and its ions. All the above investigations were non-relativistic, but after that experiments had demonstrated that such an approach was insufficient to describe the spectrum of $C^+$ (Kjeldsen et al. 1999a), $R$-matrix calculations including relativistic effects have been carried out for oxygen ions (Nahar 2004; see also Champeaux et al. 2003).

The experimental data for $N^{2+}$, $O^{3+}$ and $F^{4+}$ are compared with the data obtained using the $R$-matrix method in the middle panels of Fig. 3 (Fernley et al. 1999; Nahar & Pradhan 1997) and in Fig. 5 ($O^{3+}$: Nahar 1998, 2004) and with simulated spectra obtained using an approach based on the MCDF code by Bruneau (1984; see also above) in the lower panels of Fig. 3. Both theoretical methods are based on the configuration interaction picture but are different in many aspects. For example, the $R$-matrix method calculates *photoionization* cross sections whereas the MCDF approach predicts the *photoabsorption* cross section (in the present paper we have assumed a branching ratio of 100% towards ionization). Another limitation of the MCDF technique is that interaction between closed and open channels (i.e. between autoionizing states and continua) is not included, and as a result the resonances are

**Table 4.** Location and designation of the resonances in the photoionization spectrum of $F^{4+}$. See caption to Table 2. The peak numbers refer to Fig. 3. The accuracy of the experimental energies listed is about 200 meV.

| Peak | Energy (eV) | | | Transition |
|---|---|---|---|---|
| | Exp. | MCDF | NIST | |
| 1* | 106.05 | 105.4 | 105.97 | $2s2p(^3P)6d\ ^4D, ^4P$ |
| 2* | 108.60 | 108.0 | | $2s2p(^3P)7d\ ^4D, ^4P$ |
| 3* | 110.32 | 109.6 | | $2s2p(^3P)8d\ ^4D, ^4P$ |
| 4* | 111.43 | 110.8 | | $2s2p(^3P)9d\ ^4D, ^4P$ |
| 5 | 116.31 | 115.4 | | $2s2p(^3P)6p\ ^2P, ^2D, ^2S$ |
| 6 | 118.97 | 117.9 | | $2s2p(^3P)7p\ ^2P, ^2D$ |
| 7 | 120.83 | 118.7 | | $2s2p(^3P)8p\ ^2P, ^2D$ |
| 8 | 122.7 | 123.3 { | | $2s2p(^1P)5p^2P,^2D$<br>$2s2p(^3P)(n \geq 9)p$ |
| 9 | 127.1 | 127.9 | | $2s2p(^1P)6p\ ^2P, ^2D$ |

**Table 5.** The measured and calculated oscillator strength ($f$-values) of the $2s2p^2\ ^4P \to 2s2pnd\ ^4P, ^4D$ transitions for $N^{2+}$, $O^{3+}$, and $F^{4+}$. Exp: present experimental data; RM: $R$-matrix calculation by Fernley et al. (1999); MCDF: Multi-Configuration Dirac-Fock calculations performed as part of the present work ($N^{2+}$ and $F^{4+}$) or by Champeaux et al. (2003, $O^{3+}$).

| Transition | | Oscillator strength | | | Ratio | |
|---|---|---|---|---|---|---|
| ion | $n$ | Exp | RM | MCDF | $\frac{\text{Exp}}{\text{RM}}$ | $\frac{\text{Exp}}{\text{MCDF}}$ |
| $N^{2+}$ | 5 | 0.004126 | 0.0740 | 0.08717 | 0.06 | 0.05 |
| | 6 | 0.003079 | 0.0238 | 0.05555 | 0.13 | 0.06 |
| | 7 | 0.002656 | 0.0205 | 0.02146 | 0.13 | 0.12 |
| | 8 | 0.001437 | 0.0138 | 0.01947 | 0.10 | 0.07 |
| | 9 | 0.001076 | 0.0096 | 0.00925 | 0.11 | 0.12 |
| $O^{3+}$ | 5 | 0.002695 | 0.0704 | 0.06270 | 0.04 | 0.04 |
| | 6 | 0.002388 | 0.0374 | 0.03037 | 0.06 | 0.08 |
| | 7 | 0.002501 | 0.0223 | 0.01630 | 0.11 | 0.15 |
| | 8 | 0.002241 | 0.0145 | 0.00955 | 0.15 | 0.23 |
| | 9 | 0.001998 | 0.0100 | 0.00571 | 0.20 | 0.35 |
| | 10 | 0.001206 | 0.0070 | 0.00566 | 0.17 | 0.21 |
| $F^{4+}$ | 6 | 0.004945 | 0.0724 | 0.04480 | 0.07 | 0.11 |
| | 7 | 0.002717 | 0.0379 | 0.02566 | 0.07 | 0.11 |
| | 8 | 0.002055 | 0.0227 | 0.01642 | 0.09 | 0.13 |
| | 9 | 0.002247 | 0.0151 | 0.03253 | 0.15 | 0.07 |

assumed to have a Lorentzian line shape rather than a Fano profile. On the other hand, the MCDF approach has the advantage that it provides information concerning the identity of the peaks straightforwardly.

It can be observed from Figs. 3 and 5 that the *R*-matrix methods (except Nahar 2004; see below) are able to reproduce the magnitude of the continuum cross sections within the experimental error, but not the details of the spectral structures. In particular, the *R*-matrix calculation from the Opacity Project by Fernley et al. (1999) does not even reproduce the main features correctly in the cases of $O^{3+}$ and $F^{4+}$. For $N^{2+}$, on the other hand, the calculations (Fernley et al. 1999; Nahar 1998) are in better agreement. As for the other ions, the 2s2p($^3$P)*n*p $^2$P resonances and the peaks below the ground-state ionization thresholds are not present as the calculations do not include relativistic effects, and some of the peaks differ in intensity and are shifted in energy, but overall there is fairly good agreement between the experimental data and both *R*-matrix calculations. In the case of $O^{3+}$ the two calculations by Nahar (1998, 2004, shown in Fig. 5) represent a significant improvement compared to the Opacity Project data (Fernley et al. 1999, Fig. 3), see also (Champeaux et al. 2003). With respect to the spectral structure the best agreement with the experimental data is observed for the newer relativistic (Breit-Pauli) *R*-matrix calculation (Nahar 2004), which even reproduces the peaks below the ground-state ionization threshold with some accuracy. However, this calculation does not reproduce the magnitude of the continuum cross section correctly, in contrast to the other calculations. It underestimates it below the 2s2p $^3$P limit at 86.6 eV and overestimates it above that limit.

The MCDF description of the cross sections is generally fairly good for the gross features but fails to describe many details correctly. The peaks are shifted slightly in energy by up to ±1 eV, as already discussed. In the case of $N^{2+}$, the peak of significant intensity at 47.15 eV is an artefact resulting from the fact that the 2s2p($^1$P)3p level is incorrectly calculated to be above the ionization threshold. The $n = 4$ member for the same series is predicted at 55.5 eV and indeed is present in the experimental data, but its strength is largely overestimated in the calculation. As discussed above, the overestimation of the intensity of the 2s2p($^1$P)*n*p series can be attributed to a incorrect description of the configuration interaction between the 2s2p($^3$P)*n*p and 2s2p($^1$P)*n*p series. Most of the discrepancies occur in the case of $O^{3+}$ with regards to both the number and relative intensities of resonances. The energy region from around 77–85 eV is rather difficult to handle theoretically because of configuration interaction between the 2s2p($^3$P, $^1$P)*n*p configurations and is further complicated by the presence of doubly-excited states. The calculation shows a dip in the cross section right below the $O^{3+}$ 2s2p $^3$P limit at 86.6 eV (see Table 1) which is artificially produced by the limited number of Rydberg terms introduced in the description of the 2s2p($^3$P)*n*p series. The MCDF calculation for $F^{4+}$ looks relatively good. A double-peak appears around 115 eV because the threshold energy is calculated too low, thereby allowing the autoionization of the 2s2p($^1$P)4p levels.

In view of the number of discrepancies present it is evident that the photoionization cross section of B-like ions and in particular $O^{3+}$ constitute an important probe for benchmarking state-of-the-art calculations. Therefore, more detailed experimental data combined with new calculations are highly desirable.

### 4.2. Be-like ions: $N^{3+}$ and $O^{4+}$

The absolute cross sections for the Be-like ions $N^{3+}$ and $O^{4+}$ have been measured as part of the present project and are displayed in Fig. 6. Relative data on $O^{4+}$ have previously been obtained with a comparable resolution (Champeaux et al. 2003), and high-resolution absolute measurements have been reported for $C^{2+}$ (Müller et al. 2002) and $B^+$ (Schippers et al. 2003).

The experimental data are shown in the upper panels of Fig. 6 along with results from the OPACITY project by Tully et al. (1990, middle panels) and MCDF calculations (lower panels). As for the B-like ions, the theoretical cross sections have been convoluted with a Gaussian profile representing the experimental broadening (230 meV and 250 meV *FWMH* for $N^{3+}$ and $O^{4+}$, respectively) and are calculated as the sum of the ground state and metastable contributions, weighted by their relative abundance. Each of the experimental spectra shows two onsets (at 69.96 and 77.1 eV for $N^{3+}$ and at 113.63 eV and 103.50 eV for $O^{4+}$) which correspond to the thresholds for ionization from the $1s^22s^2$ $^1$S ground term and the $1s^22s2p$ $^3$P metastable term, respectively. The experimental ionization potentials are in close agreement with the values reported at NIST (1999) as can be seen in Table 6. By comparing the continuum contribution from the metastable component with the results of the MCDF calculations, it was estimated that 35% of the $N^{3+}$ target ions were produced in the metastable states, with the corresponding figure being 50% in the case of $O^{4+}$. The latter is identical to the value reported by Champeaux et al. (2003) who used the same ion source.

The most pronounced Rydberg series are due to the 2s2p $^3\mathrm{P} \rightarrow 2p\mathit{n}p$ $^3$D, $^3$S, $^3$P transitions from the metastable states and $2s^2$ $^1\mathrm{S} \rightarrow 2p\mathit{n}d$ $^1$P two-electron transitions from the ground state. Tables 7 and 8 display the assignments of the observed peaks and compare the experimental excitation energies with the values calculated (MCDF) and listed in NIST (1999).

The measured magnitude of the continuum cross sections is reproduced correctly by the *R*-matrix calculation of Tully et al. (1990). The data also describe the positions of the resonances fairly well but not their relative intensities. We believe that the latter is due to the employment of a too coarse energy grid in the calculation. The same problem has been observed in several other cases (see e.g. Kjeldsen et al. 2002b), and for comparison Schippers et al. (2003) used an energy grid of $13.6 \times 10^{-6}$ eV in their *R*-matrix calculation for the isoelectronic $B^+$ ion and observed excellent agreement with their experimental data. The more recent relativistic *R*-matrix results presented by Nahar (2004) slightly improve the description of the $1s^22p\mathit{n}p$ resonances in the case of $O^{4+}$ but also exhibit strange variations between the intensity of the peaks.

The MCDF calculations describe the resonance structures very well even though the absolute values differ in some cases. The magnitude of the continuum cross section is reproduced

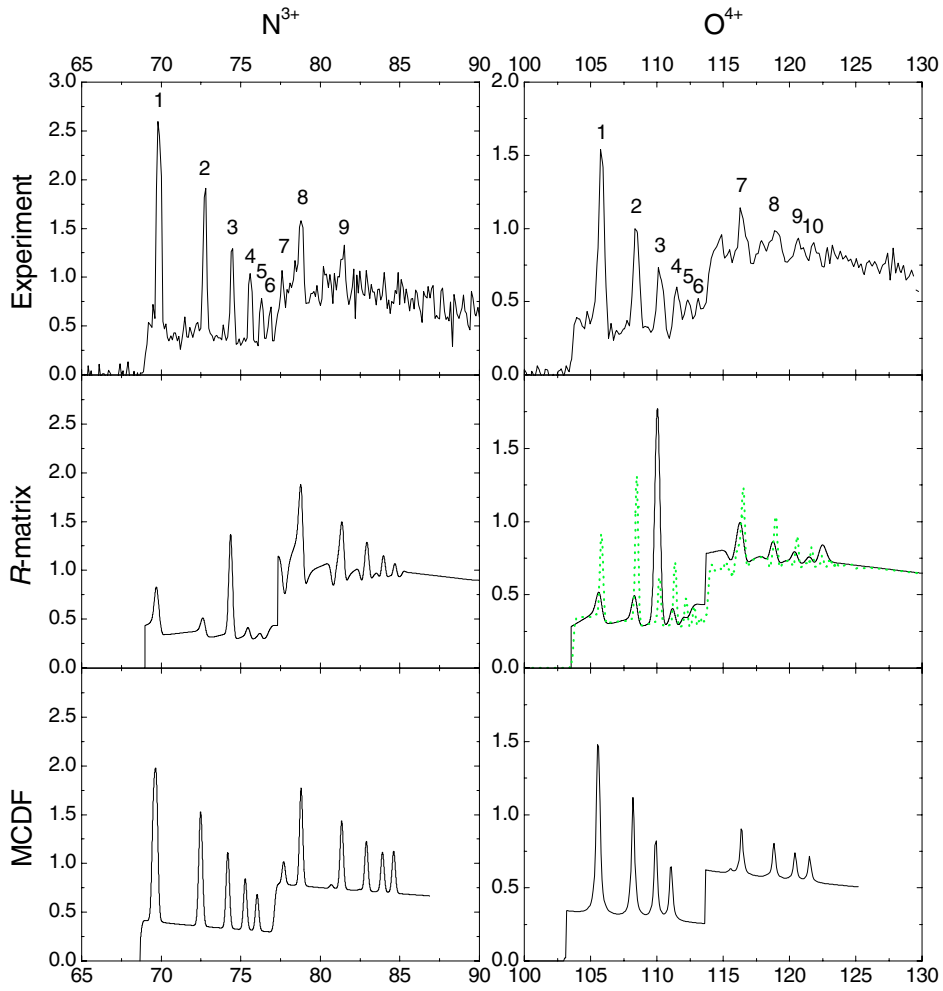


**Fig. 6.** The absolute photoionization cross sections (in Mb = $10^{-18}$ cm$^2$) as a function of the photon energy (eV) for the Be-like ions $N^{3+}$ (*left*), $O^{4+}$ (*right*). *Top*: present experimental data; *middle*: *R*-matrix calculations; *bottom*: MCDF calculations. The *R*-matrix data are by Tully et al. (solid (black) line, 1990, obtained from the Opacity Projects TOPbase) with newer data by Nahar (2004, dotted (green) line) and the MCDF data are part of the present work ($N^{3+}$) or by Champeaux et al. (2003, $O^{4+}$). The theoretical spectra have been convoluted with Gaussian distributions of 230 and 250 meV (*FWHM*), respectively, and are calculated under the assumption of a ($^3$P:$^1$P) fraction of (0.35:0.65) for $N^{3+}$ and (0.50:0.50) for $O^{4+}$. The numbers refer to Tables 7 and 8.

**Table 6.** Some relevant energy levels and ionization potentials (in eV) from our MCDF calculations and from NIST (1999) for Be-like ions. The energy of each term is obtained as the mean of the energy levels weighted statistically.

| | $N^{3+}$ | | $O^{4+}$ | |
|---|---|---|---|---|
| Level | MCDF | NIST | MCDF | NIST |
| $2s^2\ ^1S$ | 0 | 0 | 0 | 0 |
| $2s2p^2\ ^3P$ | 8.43 | 8.35 | 10.27 | 10.19 |
| $E_{IP}$ ($2s\ ^2S$) | 77.13 | 77.47 | 113.54 | 113.90 |
| $E_{IP}$ ($2s2p\ ^2P$) | | 87.47 | 125.65 | 125.88 |

relatively accurately for $N^{3+}$ but is smaller than the measured one for $O^{4+}$ by as much as 35% at 125 eV. For $N^{3+}$ the strength of the resonances is slightly underestimated for the metastable part of the spectra.

The peak No. 7 (see Fig. 6) just above the ground-state ionization threshold of the $N^{3+}$ ion is identified in Table 7 as being due to the $2s^2\ ^1S \rightarrow 2p5s\ ^1P$ two-electron transition. In fact, the *R*-matrix calculation by Tully et al. (1990) displays window resonances on the low energy side of the $2s^2\ ^1S \rightarrow 2pnd\ ^1P$ resonances which is probably associated with the 2pns series. Therefore, the excitation energy of the $2p5s\ ^1P$ resonance must be associated with the position of the dip observed at 77.9 eV in the experimental spectrum, which is in good agreement with the NIST (1999) and MCDF values.

### 4.3. C-like ions: $F^{3+}$ and $Ne^{4+}$

The present investigations include the experimental results for $F^{3+}$ and $Ne^{4+}$ shown in Figs. 7 and 8. These complement the previous photoionization cross-section measurements of the carbon-like ions $N^+$ (Kjeldsen et al. 2002a) and $O^{2+}$ (Champeaux et al. 2003). The analysis of the spectral structure of the ions is complicated by the population of several metastable states in the target ion beams and by the large number of Rydberg series present. The ground state configuration

**Table 7.** Location and designation of the resonances in the photoionization spectrum of $N^{3+}$. The peak numbers refer to Fig. 6, and * denotes that the initial state of the transition belongs to the $2s2p\ ^3P$ metastable term – otherwise the initial state is the $2s^2\ ^1S$ ground state. When several terms are given the MCDF and NIST (1999) energies correspond to the mean value of the terms energy weighted by their statistical population. The accuracy of the experimental energies listed is about 50 meV.

| Peak | Energy (eV) | | | Final state |
|---|---|---|---|---|
| | Exp. | MCDF | NIST | |
| 1* | 69.85 | 69.60 | 69.90 | $2p5p\ ^3D, ^3P, ^3S$ |
| 2* | 72.75 | 72.48 | 72.73 | $2p6p\ ^3D, ^3P, ^3S$ |
| 3* | 74.45 | 74.20 | 74.47 | $2p7p\ ^3D, ^3P, ^3S$ |
| 4* | 75.59 | 75.28 | 75.60 | $2p8p\ ^3D, ^3P, ^3S$ |
| 5* | 76.31 | 76.0 | 76.35 | $2p9p\ ^3D, ^3P, ^3S$ |
| 6* | 76.85 | | 76.88 | $2p10p\ ^3D, ^3P, ^3S$ |
| 7 | 77.72 | 77.86 | 77.93 | $2p5s\ ^1P$ |
| 8 | 78.88 | 78.78 | 78.91 | $2p5d\ ^1P$ |
| 9 | 81.49 | 81.33 | 81.51 | $2p6d\ ^1P$ |

**Table 8.** Location and designation of the resonances in the photoionization spectrum of $O^{4+}$. See caption to Table 6. The accuracy of the experimental energies listed is about 100 meV.

| Peak | Energy (eV) | | | Final state |
|---|---|---|---|---|
| | Exp. | MCDF | NIST | |
| 1* | 105.84 | 105.6 | 105.9 | $2p6p\ ^3D, ^3P, ^3S$ |
| 2* | 108.44 | 108.2 | 108.5 | $2p7p\ ^3D, ^3P, ^3S$ |
| 3* | 110.21 | 109.9 | | $2p8p\ ^3D, ^3P, ^3S$ |
| 4* | 111.48 | 111.1 | | $2p9p\ ^3D, ^3P, ^3S$ |
| 5* | 112.35 | | | $2p10p\ ^3D, ^3P, ^3S$ |
| 6* | 113.12 | | | $2p11p\ ^3D, ^3P, ^3S$ |
| 7 | 116.39 | 116.39 | | $2p6d\ ^1P$ |
| 8 | 118.82 | 118.83 | | $2p7d\ ^1P$ |
| 9 | 120.60 | 120.42 | | $2p8d\ ^1P$ |
| 10 | 121.74 | 121.52 | | $2p9d\ ^1P$ |

of C-like ions, $1s^22s^22p^2$, gives rise to the $^3P$ ground state term and to the $^1D$ and $^1S$ metastable terms. All 3 terms were populated in the experimental target ion beams, and an additional small fraction was in the $1s^22s2p^3\ ^5S$ excited term. MCDF values for relevant energy levels and ionization potentials are presented in Table 9 together with the corresponding numbers from NIST (1999). We note that the MCDF energy level of the $^5S$ metastable term differs by almost 1 eV from the NIST values.

The principal dipole allowed transitions are due to $2s \rightarrow np$ excitations from the $^3P$, $^1D$ and $^1S$ terms and $2p \rightarrow nd$, $ns$ excitations from the $^5S$ term as follows:

$$2s^22p^2\ ^3P + h\nu \rightarrow 2s2p^2(^4P,^2P)np\ ^3S,^3P,^3D \quad (1)$$

$$2s^22p^2\ ^1D + h\nu \rightarrow 2s2p^2(^2D)np\ ^1P,^1D,^1F \quad (2)$$

$$2s^22p^2\ ^1S + h\nu \rightarrow 2s2p^2(^2S)np\ ^1P \quad (3)$$

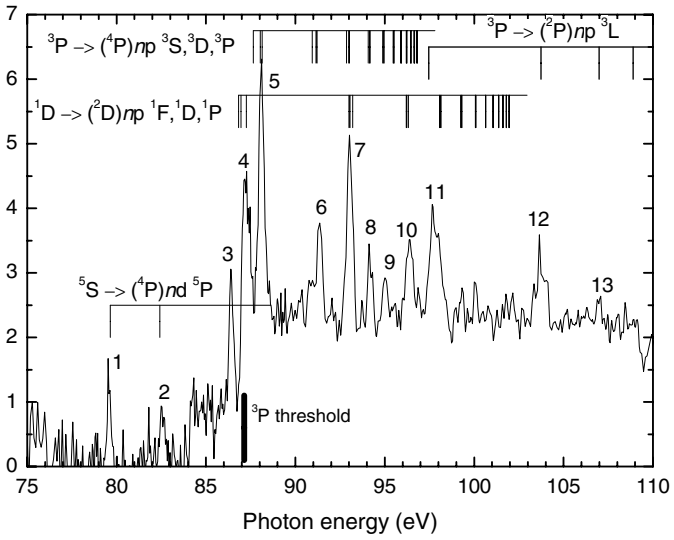


**Fig. 7.** The absolute photoionization cross sections of $F^{3+}$. The numbers refer to Table 10. The Rydberg series are extrapolated utilizing the series limits and lower-lying members with known energy (NIST 1999).

$$2s2p^3\ ^5S + h\nu \rightarrow 2s2p^2(^4P)ns, nd\ ^5P. \quad (4)$$

Coulomb autoionization of the final $^5P$ term in (4) and of the $^3S$ term in (1) is forbidden by the spin and parity selection rules, respectively. Such resonances may still be present, however, as was the case for the B-like ions. The experimental and calculated positions of the main lines observed in the experimental spectra as well as an assignment based on our MCDF calculations are given in Tables 10 and 11.

The experimental spectrum of $F^{3+}$ is shown in the left upper panel of Fig. 8 and in more detail in Fig. 7. Two peaks (No. 1 and 2) due to $2p \rightarrow (n = 6, 7)d$ transitions from the $2s2p^3\ ^5S$ metastable term are clearly visible at 79.57 eV and 82.56 eV. By comparing the strength of these lines with the MCDF calculation it is estimated that 2–3% of the target ions were in the $^5S$ term. Direct ionization from the $2p^2\ ^1D$ excited term is responsible for the sharp onset at 84.07 eV, in close agreement with the previously observed value of 84.01 eV (NIST 1999), but 1 eV above our MCDF energy threshold, see Table 9. At that energy the cross section rises to a small plateau with a magnitude of ~0.9 Mb. Using this value the $^1D$ population is determined to be 30%. There is no clear evidence of an onset at 80.50 eV which might arise due to direct ionization from the $^1S$ term, and no transitions belonging to that term have been observed. For these reasons the population of the $^1S$ term is neglected in the analysis.

It is likely that the $(^1D) \rightarrow (^2D)4p$ transitions are responsible for the partially resolved peaks 3, 4, while the $n = 5$ and 6 members of the same series contribute substantially to the peaks Nos. 7 and 10. Similarly, $(^3P) \rightarrow (^4P)(n = 5–9)p$ can be assigned to the peaks 5, 6, (7), 8, and 9 with some certainty. Finally, the peaks 11 and 12 can be attributed to $(^3P) \rightarrow (^2P)(n = 4, 5)p$.

The data for $Ne^{4+}$ (Fig. 8) provide less detailed information because they are recorded with a reduced photon-energy resolution and exhibit larger statistical fluctuations. As a result,

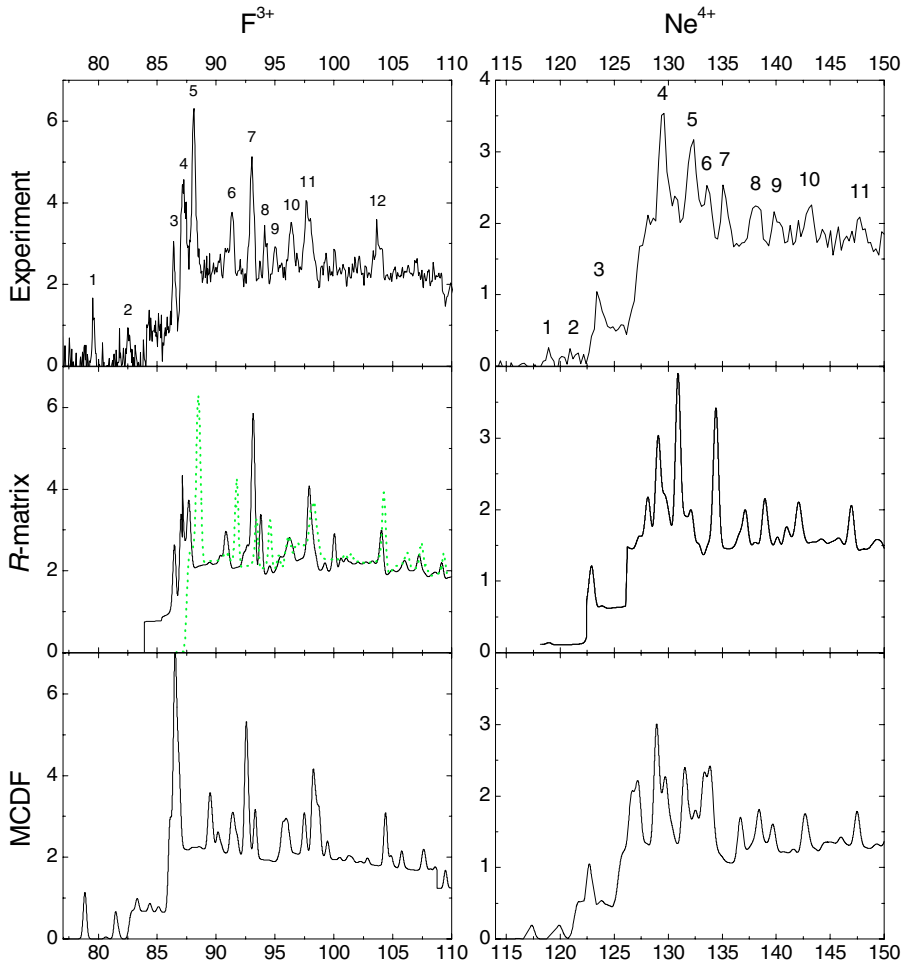


**Fig. 8.** The absolute photoionization cross sections (in Mb = $10^{-18}$ cm$^2$) as a function of the photon energy (eV) for the C-like ions $F^{3+}$ (*left*) and $Ne^{4+}$ (*right*). *Top*: present experimental data; *middle*: *R*-matrix calculations; *bottom*: MCDF calculations. The *R*-matrix data by Lou & Pradhan (1989, obtained from the Opacity Projects TOPbase) are shown by (black) solid line, whereas the data by (Nahar & Pradhan 1997, ground state only) are shown by (green) dotted line for $F^{3+}$. The theoretical spectra have been convoluted with Gaussians of 300 and 550 meV (*FWHM*), respectively, and are calculated under the assumption of a ($^3$P:$^1$D:$^1$S:$^5$S) fraction of (68:30:0:2) for $F^{3+}$ and (56:36:6:2) for $Ne^{4+}$. The MCDF data are part of the present work, and the numbers refer to Tables 10 and 11. The experimental data for $F^{3+}$ are shown enlarged in Fig. 7.

**Table 9.** Some relevant energy levels and ionization potentials (in eV) from our MCDF calculations and from NIST (1999) for C-like ions. The energy of each term is obtained as the mean of the energy levels weighted statistically.

| | $N^{3+}$ | | $O^{4+}$ | |
|---|---|---|---|---|
| Level | MCDF | NIST | MCDF | NIST |
| $2s^22p^2\ ^3P$ | 0 | 0 | 0 | 0 |
| $2s^22p^2\ ^1D$ | 3.36 | 3.13 | 4.16 | 3.76 |
| $2s^22p^2\ ^1S$ | 6.85 | 6.64 | 8.18 | 7.92 |
| $2s2p^3\ ^5S$ | 8.33 | 9.20 | 10.15 | 10.96 |
| $E_{IP}$ ($2s^22p\ ^2P$) | 86.38 | 87.14 | 125.44 | 126.22 |
| $E_{IP}$ ($2s2p^2\ ^4P$) | 96.50 | 97.82 | 137.15 | 138.72 |
| $E_{IP}$ ($2s2p^2\ ^2D$) | 105.89 | 106.09 | 148.25 | 148.41 |
| $E_{IP}$ ($2s2p^2\ ^2S$) | 111.08 | 111.64 | 154.54 | 154.84 |
| $E_{IP}$ ($2s2p^2\ ^2P$) | 114.29 | 113.82 | 157.87 | 157.22 |

only tentative assignments have been given for several peaks. Contrary to the $F^{3+}$ case a clear contribution from the $^1$S term can be identified from the peak 3, and the population of the term is determined to be 6%. By comparing with the MCDF calculations it was estimated that the $^5$S term contributed 1–2% of the target beam and the $^1$D term by 36%. The ionisation threshold of the $^1$D term is observed at 122.7(1) eV, close to the value of 122.46 eV given in NIST (1999), see Table 9. The onset of the continuum cross section observed at 127.1(1) eV corresponds to the ionisation threshold for the ions in the ground state, although it is 0.9 eV higher than the NIST value of 126.22 eV. As in the case of the B- and Be-like ions, a continuous decrease of the magnitude of the continuum cross section is seen when moving through the series $N^+$ (Kjeldsen et al. 2002a), $O^{2+}$ (Champeaux et al. 2003), $F^{3+}$, and $Ne^{4+}$, together with the expected downward movement of the Rydberg series.

The experimental cross sections are compared with simulated spectra in Fig. 8. It can be observed that the *R*-matrix calculations by Lou & Pradhan (1989, performed as part of the Opacity Project) and Nahar & Pradhan (1997, ground state

**Table 10.** Location and designation of the resonances in the photoionization spectrum of $F^{3+}$. The peak numbers refer to Figs. 8 and 7. $2s^22p^2$ or $2s2p^3$ (see Table 9) has been left out of the initial configurations as well as $2s2p^2$ from the final configurations of the transitions. When several terms are given, the MCDF and NIST (1999) energies correspond to the mean values. The accuracy of the experimental energies listed is about 100 meV.

| Peak | Energy (eV) | | | Transition |
|---|---|---|---|---|
| | Exp. | MCDF | NIST | |
| 1 | 79.57 | 78.9 | 79.67 | $^5S \rightarrow (^4P)5d\ ^5P$ |
| 2 | 82.56 | 81.7 | | $^5S \rightarrow (^4P)6d\ ^5P$ |
| 3 | 86.42 | 86.1 | | $^1D \rightarrow (^2D)4p\ ^1D$ |
| 4 | 87.26 | 86.6 | | $^1D \rightarrow (^2D)4p\ ^1F, ^1P$ |
| 5 | 88.10 | 86.5 | | $^3P \rightarrow (^4P)5p\ ^3S, ^3D, ^3P$ |
| 6 | 91.35 | 89.5 | | $^3P \rightarrow (^4P)6p\ ^3S, ^3D, ^3P$ |
| 7 | 93.04 | 92.6 | | $^1D \rightarrow (^2D)5p\ ^1F, ^1P, ^1D$ |
| | | 91.4 | | $^3P \rightarrow (^4P)7p\ ^3S, ^3D, ^3P$ |
| 8 | 94.18 | 92.6 | | $^3P \rightarrow (^4P)8p\ ^3S, ^3D, ^3P$ |
| 9 | 95.02 | 93.3 | | $^3P \rightarrow (^4P)9p\ ^3S, ^3D, ^3P$ |
| 10 | 96.39 | 95.9 | | $^1D \rightarrow (^2D)6p\ ^1F, ^1P, ^1D$ |
| 11 | 97.81 | 98.3 | | $^3P \rightarrow (^2P)4p\ ^3D, ^3P$ |
| 12 | 103.72 | 104.4 | | $^3P \rightarrow (^2P)5p\ ^3D, ^3P$ |

**Table 11.** Location and designation of the resonances in the photoionization spectrum of $Ne^{4+}$. See caption to Table 10. The assignments should be regarded as tentative. The accuracy of the experimental energies listed is about 200 meV.

| Peak | Energy (eV) | | Final state |
|---|---|---|---|
| | Exp. | MCDF | |
| 1 | 118.8 | 117.37 | $^5S \rightarrow (^4P)6d\ ^5P$ |
| 2 | 121.2 | 119.97 | $^5S \rightarrow (^4P)7d\ (^5P)$ |
| 3 | 123.55 | 125.41 | $^1S \rightarrow (^2D, ^2P)5p\ ^1P$ |
| 4 | 129.48 | 130.4 | $^1D \rightarrow (^2S)4p\ ^1P$ |
| | | 129.4 | $^1D \rightarrow (^2D)5p\ ^1P, ^1D, ^1F$ |
| | | 129.8 | $^2P \rightarrow (^4P)7p\ ^3D, ^3P$ |
| 5 | 132.22 | 133.5 | $^2P \rightarrow (^2P)4p\ ^3D, ^3P$ |
| 6 | 133.55 | 133.3 | $^2P \rightarrow (^2D)5p\ ^3D, ^3P$ |
| | | 132.2 | $^2P \rightarrow (^4P)8p\ ^3D, ^3P$ |
| | | 134.0 | $^1D \rightarrow (^2D)6p\ ^1P, ^1D, ^1F$ |
| 7 | 135.20 | 136.6 | $^1D \rightarrow (^2S)5p\ ^1P$ |
| 8 | 138.10 | 138.0 | $^2P \rightarrow (^2D)6p\ ^3D, ^3P$ |
| 9 | 140.04 | 140.2 | $^1D \rightarrow (^2S)6p\ ^1P$ |
| 10 | 143.06 | 142.9 | $^3P \rightarrow (^2P)5p\ ^3D, ^3P$ |
| 11 | 147.8 | 147.7 | $^3P \rightarrow (^2P)6p\ ^3D, ^3P$ |

only) reproduce the main features of the experimental data. The best agreement is found in the case of $F^{3+}$. The calculations evidently fail to reproduce the peaks from the $^5S$ term since these occur as the result of relativistic effects and the calculations are non-relativistic. These lines are well reproduced in the MCDF results, but this method only reproduces the main structures above the $^3P$ threshold approximately correctly. The calculated magnitude of the cross sections is within the experimental uncertainty, except that in the MCDF case the continuum cross sections for $Ne^{4+}$ is underestimated as it was observed above for $O^{4+}$.

It is difficult to judge the accuracy of the calculated data with respect to the spectral structure for $Ne^{4+}$ due to the large photon-energy bandwidth involved in the experiment and the large number of Rydberg series present. In the energy region investigated at least five groups of overlapping Rydberg series converging to four different $Ne^{5+}$ ionisation thresholds are present. Agreement between theory and experiment is only evident below the ground-state threshold where the $^1D$ plateau with the prominent peak is reproduced in both the OPACITY (Lou & Pradhan 1989) and the MCDF data. Above the ionisation threshold of the ground state, many discrepancies with respect to the spectral structure occur between the experimental data and both calculations, perhaps most pronounced in the case of MCDF. A tentative assignment of the observed peaks is given in Table 11.

### *4.4. Comparison with the model functions by Verner et al. (1996)*

For the sake of simplicity, models of photoionised plasmas often utilize analytical model functions (see e.g. Verner et al. 1996, and references therein) to describe the photoionisation cross section, rather than large data sets. This procedure makes the models more simple, but the cost is that no information concerning the spectral structure is included. The present experimental data and the model functions provided by Verner et al. (1996) generally exhibit good agreement with respect to the magnitude of the continuum cross sections. In most case the differences are less than 10%, but for $N^{3+}$ the Verner data are about 20% larger than the experimental ones.

## 5. Concluding remarks

Absolute cross sections for photoionisation of important members of the beryllium, boron and carbon iso-electronic sequences have been measured, analysed and compared with theoretical results of the *R*-matrix and the MCDF methods. In most cases it has been possible to characterize the spectral features on the basis of the results of the MCDF calculations, although the population of metastable components in the experiments made the analysis more complicated. In general, good agreement is observed for the magnitude of the cross sections, whereas very significant differences concerning the spectral structures are present, in particular for the highest charged ions. We note that good agreement between experimental data and *R*-matrix calculations from the Opacity Project previously has been observed for some singly charged ions in the same region of the periodic table. Thus, it is evident that the accuracy of the data of the Opacity Project exhibit large variations from one atomic species to another and that their reliability cannot be judged in general terms. For the ions investigated in this manuscript, further investigations are highly desirable. These should be based on better-resolved experimental data as well as more accurate calculations, such as those previously performed

for e.g. $B^+$ (Schippers et al. 2003, and references therein) and $C^+$ (Kjeldsen et al. 1999a, 2001; Yu Yan & Seaton 1987; Nahar & Pradhan 1997; Nahar 2002).

*Acknowledgements.* We would like to acknowledge the support of the Aarhus Centre for Atomic Physics (ACAP), funded by the Danish Basic Research Foundation, and of the European Community – Access to Research Infrastructure action of the Improving Human Potential Programme. We are grateful to the staff of the Institute for Storage Ring Facilities (ISA) at the University of Aarhus for their assistance throughout the project.

## References

Aguilar, A., Covington, A. M., Hinojosa, G., et al. 2003, ApJS, 146, 467
Berrington, K. A., Burke, P. G., Dufton, P. L., & Kingston, A. E. 1977, J. Phys. B, 10, 1465
Bizau, J.-M., Cubaynes, et al. 2000, Phys. Rev. Lett., 84, 435
Bizau, J.-M., Cubaynes, D., Esteva, J.-M., et al. 2001, Phys. Rev. Lett., 87, 273002
Bizau, J.-M., Bouisset, E., Blancard, C., et al. 2003, Nucl. Instrum. Meth. B, 205, 290
Bizau, J.-M., Champeaux, J.-P., Cubaynes, D., et al. 2004, Phys. Scr., 110, 57
Bruneau, J. 1984, J. Phys. B, 17, 3009
Champeaux, J.-P., Bizau, J.-M., Cubaynes, D., et al. 2003, ApJS, 148, 583
Covington, A. M., Aguilar, A., Covington, I. R., et al. 2001, Phys. Rev. Lett., 87, 243002
Covington, A. M., Aguilar, A., Covington, I. R., et al. 2002, Phys. Rev. A, 66, 062710
Cunto, W., Mendoza, C., Ochsenbein, F., & Zeippen, C. J. 1993, A&A, 275, L5
Domke, M., Schultz, K., Remmers, G., Kaindl, G., & Wintgen, D. 1996, Phys. Rev. A, 53, 1424
Fernley, J. A., Hibbert, A., Kingston, A. E., & Seaton, M. J. 1999, J. Phys. B: Atomic, Molecular and Optical Physics, 32, 5507
Kjeldsen, H., Folkmann, F., Hansen, J. E., et al. 1999a, ApJ, 524, L146
Kjeldsen, H., Folkmann, F., Knudsen, H., et al. 1999b, J. Phys. B, 32, 4457
Kjeldsen, H., Folkmann, F., Hansen, J. E., et al. 2001, ApJS, 135, 53193
Kjeldsen, H., Kristensen, B., Brooks, R. L., et al. 2002a, ApJS, 138, 219
Kjeldsen, H., Kristensen, B., Folkmann, F., & Andersen, T. 2002b, J. Phys. B, 35, 3655
Kjeldsen, H., Folkmann, F., Jacobsen, T. S., & West, J. B. 2004, Phys. Rev. A, 69, 050501(R)
Kjeldsen, H., Folkmann, F., van Elp, J., et al. 2005, Nucl. Instr. Meth. B, in press
Koizumi, T., Itoh, Y., Sano, M., et al. 1995, J. Phys. B, 28, 609
Lou, D., & Pradhan, A. K. 1989, J. Phys. B, 22, 3377
Lyon, I. C., Peart, B., West, J. B., & Dolder, K. 1986, J. Phys. B, 19, 4137
Msezane, A., Reilman, R. F., Manson, S. T., Swanson, J. R., & Armstrong, J. L. 1977, Phys. Rev. A, 13, 668
Müller, A., Phaneuf, R. A., Aguilar, A., et al. 2002, J. Phys. B, 35, L137
Nahar, S. N. 1998, Phys. Rev. A, 58, 3766
Nahar, S. N. 2002, Phys. Rev. A, 65, 052702
Nahar, S. N. 2004, Phys. Rev. A, 69, 042714
Nahar, S. N., & Pradhan, A. K. 1997, ApJS, 111, 339, data downloaded from `ftp.astronomy.ohio-state.edu`
NIST 1999, The NIST Atomic Spectra Database, version 2.0, `http://physics.nist.gov/`
Schippers, S., Müller, A., McLaughlin, B. M., et al. 2003, J. Phys. B, 36, 3371
Seaton, M. 1987, J. Phys. B, 20, 6363
Sobelman, I. I. 1992, Atomic Spectra and Radiative Transitions (Berlin, Germany: Springer-Verlag)
The Opacity Project Team 1995, The Opacity Project, Vol. 1 (Briston, UK: Institute of Physics Publishing)
Tully, J. A., Seaton, M. J., & Berrington, K. A. 1990, J. Phys. B, 23, 3811
Verner, D. A., Ferland, G. J., Korista, K. T., & Yakovlev, D. G. 1996, ApJ, 465, 487
West, J. B. 2001, J. Phys. B, 34, 45
Yamaoka, H., Oura, M., Kawatsura, K., et al. 2002, Phys. Rev. A, 65, 012709
Yu Yan, & Seaton, M. J. 1987, J. Phys. B, 20, 6409